Engineering and Technology Journal e-ISSN: 2456-3358

Volume 10 Issue 08 August-2025, Page No.-6112-6124

DOI: 10.47191/etj/v10i08.09, I.F. – 8.482

Ripple Correlation Control for Real-Time Optimization in Photovoltaic Systems and Switched Reluctance Motors

Ahmed Ibrahim Khudhur Khudhur[1], Abbas UĞURENVER[2]

[1,2]Department of Electrical and Electronics Engineering, Istanbul Aydin University, Institute of Graduate Studies

ABSTRACT: Ripple Correlation Control (RCC) is an actual time optimization method that utilizes the inherent switching ripple of electrical electronic systems to enhance a cost function associated with system states. In solar energy (PV) applications, RCC is used to optimize output power by choosing a cost function that precisely represents the panel's power characteristics. While the global maximum is theoretically unique (unimodal), practical considerations such as partial shading might create many peaks, necessitating mode-switching tactics to improve the likelihood of reaching the global optimum. RCC is especially advantageous for switching power converters, since the intrinsic ripple in system variables ensures continuous excitation. This property enables RCC to ascertain the gradient direction autonomously, eliminating the necessity for external perturbation, thereby rendering it appropriate for maximum power point tracking (MPPT) in photovoltaic systems and efficiency enhancement in motor drives. In motor applications, RCC is incorporated in Proportional-Integral-Derivative (PID) controllers to augment the performance of Switched Reluctance Motors (SRMs). The PID controller improves system stability and reduces steady-state error and oscillations. Nevertheless, while the integral component enhances precision, it may compromise transient performance and velocity. The derivative component, on the other hand, enhances responsiveness and aids in mistake forecasting. The parametric input/output (PID) controller is tuned using procedures such as Ziegler - Nichols to guarantee optimum dynamic response. Switched Reluctance Motors (SRMs) are increasingly favoured for their robust design and intrinsic fault tolerance, mostly attributed to the independent torque production throughout phases and the lack of permanent magnets. These characteristics render SRMs impervious to common converter malfunctions like shoot-through incidents. Nonetheless, SRM torque generation is markedly nonlinear, affected by rotor position and phase current, posing difficulties for traditional control methods. Current fault-tolerant techniques for SRMs, like present profiling and healthy phase extension, mostly rely on static, offline data and do not accommodate dynamic variations in machine parameters. Moreover, several approaches are constrained to low-speed operation and have difficulties in sustaining torque production with little ripple during fault situations. Combining RCC with adaptable control methods such as PID, particularly in dynamic settings, may improve system performance in solar power plants and electrical motor drives, providing a robust and economical management strategy to feed real-time, nonlinear systems.

KEYWORDS: RCC, PV, MPPT, P&O, SRM, PID

I. INTRODUCTION

Photovoltaic (PV) systems are crucial for attaining national objectives concerning energy independence and alleviating the adverse environmental effects of elevated carbon emissions. In the absence of maximum power point tracking (MPPT), photovoltaic systems cannot consistently attain their theoretical maximum electrical capacity due to variations in sun radiation and ambient temperature. Maximum Power Point Tracking technologies are engineered to allow solar systems to adjust to environmental variations, hence enhancing electricity supply efficiency. Maximum Power Point Tracking methods are generally incorporated into power electronic conversion systems, wherein the converter's duty cycle is adjusted to improve output efficiency. At this point, the load has reached the maximum power that is possible [1], [2]. It has been determined via research that a number of different MPPT algorithms are used. [3], [4], and [5] The P&O technique is the most important algorithm. In order to continuously track the fluctuations in voltage of the arrays and, as a consequence, assess the associated changes in output power, this technology does need additional control circuits to be implemented. Due to the fact that it forces the system to fluctuate regarding the maximum power point (MPP) rather of continually following it, the P&O algorithm, despite its economic efficiency and simplicity, demonstrates inefficiencies in steady state conditions. Because it is unable to discern between power changes that are caused by external variables and those that are the consequence of internal algorithmic disturbances, the P&O algorithm proves to be effective in dynamic environmental conditions [6]. Maximum power point tracking (MPPT) is an important technique because of the quadratic current and voltage (I-V) features of solar panels, as well as the changes that are brought about by aging, temperature, and exposure to sunlight [7], [8]. For a maximum power point tracking (MPPT) approach to be effective, it is necessary to have accurate measurements of the power that is being fed into the converter, as well as sufficient accuracy in the control of the converter. Main nonlinear current and voltage (I-V) properties of solar panels, as well as the changes in panel parameters that are induced by many variables such as exposure to sunlight, temperature, and aging, are the reasons why maximum power point tracking (MPPT) is necessary. An effective maximum power point tracking (MPPT) system requires accurate measurement of the power that is sent into the converter, as well as appropriate precision in the control of the converter. As a method for system improvement in the face of persistent oscillations, Ripple Correlation Control (RCC) is shown to be both successful and flexible over time [9]. A Maximum Power Point (MPP) is successfully accomplished by the use of this technique by evaluating the characteristics of the circuit at two distinct moments during the usual switching ripple. When the delay is associated with the calculation of the mean switching ripple is eliminated. When it comes to control, RCC is considered to be a kind of outlier-seeking control, which means that it is reliant on the internal system variations rather than the outside influences [10], [11]. For stationary digital applications, the RCC technique has been shown to be reliable [12]. This research enhances the theoretical foundation of digital ripple correlation control (DDRCC) [13] and demonstrates its relevance to system ripples caused by PWM, resulting in ultra-fast PV Maximum Power Point Tracking (MPPT) and resolution in MPPT systems using patch PWM control. The RCC technique has proven effective as a quick and accurate solution for photoelectric maximum power point tracking (MPPT). Nevertheless, the existing implementations of the RCC have used ripple created by the switching transformer rather than rippling produced by the ripple itself, as shown in this paper. In a digital implementation of RCC, power is measured throughout transitions in the switching waveform rather than the ripple waveform [12]. Achieving RCC at the switching frequency guarantees excellent tracking velocity, since the panel's operating point may be modified with each switching cycle. Nonetheless, the MPP monitoring frequency correlates with the changing frequency, and its implementation may provide difficulties. Analysis of Figure. 4 reveals that for panel currents below the MPP current, fluctuations in power and current will transpire simultaneously. Conversely, above the MPP, fluctuations in power and current will demonstrate a phase difference of 180°. The relationship between the phase distribution of power and current perturbation is essential for the efficient functioning of the RCC technique. Furthermore, by using RCC to mitigate the ripple induced by dithering, DDRCC circumvents the switching frequency constraints imposed by RCC [14]. The primary contribution of this work is a novel control mechanism that facilitates both high tracking efficiency and rapid dynamic reaction in photovoltaic maximum power point tracking systems. The essential comprehension is to use the data from the PWM dither ripple for rapid and precise tracking. The suggested technique achieves a tenfold increase in tracking speed while preserving tracking efficiency relative to standard perturbation and observation (P&O) implementation. Conversely, at the identical tracking velocity, the suggested control mechanism results in a substantial reduction in losses attributable to tracking mistakes as compared to traditional P&O. Furthermore, the proposed DDRCC approach mitigates several issues associated with current PV RCC methods, which have hindered the widespread deployment of RCC thus far [14]. DDRCC technology is specifically engineered for cost-effective or low-energy applications, including PV module-integrated converters for electricity and mobile solar energy systems. The suggested two-tier controller design could decrease the level of complexity of system management, with RCC primarily managing the "slow" dynamic and MRAC regulating the "fast" dynamics. Prior research has confirmed the reliability of RCC and MRAC, correspondingly. The integration of two stable subsystem does not guarantee the overall stability of the system. A prevalent issue with algorithms that use MPPT is the transitory fluctuations in the system's final voltage after an abrupt alteration in the duty cycle to pursue the maximum power point[15].

Thus, the ideal MPPT control system must be simple, economical, and demonstrate rapid convergence to the MPP while maintaining little output voltage oscillation. This paper introduces a dual-layer MPPT control methodology, utilizing ripple correlation control (RCC)[16],[17],[18],[19] in the first layer and model reference adaptive control (MRAC) in the second layer. The switching reluctance motor (SRM) is an electric motor drive that produces torque by the magnetic attraction between stator electromagnets and a corresponding salient pole [20],[21]. Poles are positioned on the rotor. The rotor consists exclusively of ferromagnetic material. In a Switched Reluctance Motor (SRM), the stator comprises just windings, whilst the rotor is devoid of windings, leading to less power loss and enhanced torque. Thus, the torque produced is due to the alignment inclinations of the stator and rotor poles [22]. The effectiveness of speed performance is essential for the dependability of SRM drives. The Proportional Integral Derivative (PID) controller is commonly utilized as the speed regulator in AC motor drives, recognized for its swift transient response and adequate steady-state performance [23],[24]. Nevertheless, the PID controller is generally vulnerable to alterations in the performance of the drive is therefore hindered by factors such as motor characteristics, non-linearity in the system, load disturbances, and various speed fluctuations [25], [26].The remarkable efficiency, strong reliability, and minimal maintenance requirements of brushless permanent magnet direct current (BLPMDC) motors have garnered significant interest [27–31]. These motors have become prominent and are employed in various applications, including aerospace, commercial, and residential sectors. These applications often necessitate a motor that is reliable and has excellent power density and efficiency [32–36]. BLPMDC motors, without rotor windings, employ electrical commutation instead of mechanical commutation, enabling them to be driven by a power electronic converter or inverter [37–41]. A suitable speed controller is essential for optimal motor performance. The three primary types of speed controllers for BLPMDC motors are positioning controllers, variable load controllers, and open-loop speed control (constant load) [42–46]. The development of an effective BLPMDC motor controller has been thoroughly recorded in numerous literary sources. [47] conducted a comprehensive comparison of two-speed control approaches for BLPMDC motors: a conventional PID controller and an optimal autotuning PID controller. The motor characteristics were initially determined through experimentation and subsequently employed in MATLAB simulations to attain optimal performance. The auto-tuning controller exhibited its capacity to achieve the target speed while reducing torque and current variations. A filtered closed-loop speed controller for both counterclockwise and clockwise motion, built in MATLAB/Simulink, was examined in [48]. The controller was evaluated at various speeds. The results confirmed the efficacy of the proposed controller. Similarly, [49] employed and contrasted with two speed control strategies: modified reference adaptive control and self-tuned PID. The choice of control is determined by the equilibrium between the modified model-reference adaptive control and the PID in this approach. The latter strategy was more effective than the former. A comparison of conventional and digital PI controllers for BLPMDC motors was conducted in [50]. Both techniques employed PWM-based controls. The simulated results were corroborated by the experimental data. The digital controller demonstrated swift response time and an uncomplicated control mechanism. The digital controller is an excellent choice when the disruption in the torque/speed profile is limited due to its capabilities. Additionally, References [51–54] conducted a comparative examination of P and PI controllers for the BLPMDC motor. A mathematical model of the motor was established, and motor driving models were constructed with MATLAB/SIMULINK. The PI controller showed effectiveness in reducing overshoot and correcting steady-state errors. The MOSFET bridge's switching sequences were regulated by a current controller employing a PID setup for the BLPMDC motor, as demonstrated in References [52-56]. The velocity could be regulated by modifying the current. The newly presented controller was assessed against the conventional PI and PID speed controllers. The PID controller was identified as the most effective compared to other controllers. For optimal motor performance, the driving system must be efficient. PI and PID controllers are frequently employed to control the speed of electric motors due to their straightforward designs and implementations. ability to mitigate the effects of parameter fluctuations and robust velocity monitoring capabilities. PI and PID controllers are clearly uncomplicated, despite their cost-effectiveness and simplicity.

II. RIPPLE CORRELATION CONTROL (RCC)

Ripple Correlation Control is a complex optimization method designed for real-time applications. Identifying phases and cost functions which involve ripples will provide sufficient information to determine the optimal operating point. RCC specializes in switching power converters, where the switching action perpetually engages the states and generates ripples. RCC has been suggested for motor driving applications. The energy stored in the motor's magnetism may mitigate the oscillations produced by the primary switching components. A second ripple term at an appropriate frequency range may be included to provide the required nonzero signal. Alternative observer-based systems that generate indicators for the Ripple Correlation Control legislation are probably feasible. The RCC delineates the duty cycle that ensures the load consistently obtains optimal electricity in a stable state. The primary innovation of RCC lies in exploiting the converter's inherent switching disturbance to disturb the system and then evaluate the Maximum Power Point (MPP) [19]. The RCC constitutes an advanced iteration of the P&O approach [3],[4],[5], incorporating the perturbation intrinsic to the converter. The elimination of the need for outside circuits to generate disruption is one of the factors that contributes to the benefits of this technology. In addition to this, RCC has shown asymptotic resolution for the MPP while minimizing the complexity of the controller and carrying out the circuit setup in a transparent manner [19]. The RCC is a result of the discovery that the median of the temporal fluctuations of the array's electrical voltages serves as the foundation for the RCC. This development is what gives origin to the RCC (v_{pV}) and power (p_{pV}) is positive to the left of the MPP, negative to the right of the MPP, and exactly zero at the MPP see as Figure. 1.

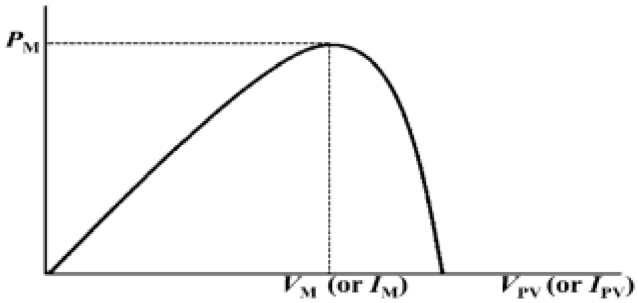

FIGURE. 1. Characteristics between Power and voltage of (PV) systems.

A cost function $(\mathcal{J})$ that is dependent on a state variable (z) is optimized via backdrop Ripple Correlation Control (RCC), which makes use of switching ripples in order to achieve this optimization. Assume that the objective is to locate a cost function that appropriately depicts panels power and to maximize ($\mathcal{J}$), that is employed in an MPPT application for a photovoltaic panel. Through the use of a sign change, it is possible to develop a comparable formulation in order to minimize a cost function, such as optimizing efficiency (minimizing power loss). In order to maintain global stability, it is necessary for ($\mathcal{J}$) to be unimodal, which indicates the existence of a single global maximum. In the context of a real solar the application, local shadowing has the potential to generate a large number of peaks [88], so the mode-switching approach enhances the possibility of reaching the global maximum intensity. The greatest value is attained given a suitable cost function $\mathcal{J}(z)$.

$$\frac{d\mathcal{J}}{dz} = 0. \quad (1)$$

There is an input at the power conversion facility, which may be shown by the duty cycle in a direct current to direct current converter. Given that ($\mathcal{J}$) needs to be unimodal, the value of the steady state

$$\varphi(u) = \lim_{t\to\infty} z(u,t) \quad (2)$$

must exhibit monotonicity across the operational range. Monotonicity guarantees the absence of polarity inversion in the system gain and can be achieved through constraints or a coordinate transformation. A fundamental control law

$$u = k\int \frac{d\mathcal{J}}{dz}\,dt \quad (3)$$

will optimize the operating point to achieve the greatest value of ($\mathcal{J}$). The sign (k) and effect of u on z deciding whether the control law approaches a maximum or a minimum. The magnitude of (k) affects the rate of convergence. Typically, derivatives are dJ/dz not accessible in actual systems, necessitating the employment of a more effective controller. There is no change in the equilibrium point of operation regardless of whether the integrator of (3) is multiplied by a positive number or not. A multiplier that is beneficial is$\left(dz/dt\right)^2$ which, by applying the chain rule, produces

$$u = k\int \frac{d\mathcal{J}}{dz}\frac{dz}{dt}\frac{dz}{dt}\,dt = k\int \frac{d\mathcal{J}}{dt}\frac{dz}{dt}\,dt \quad (4)$$

$$\frac{d\mathcal{P}pv}{dt}\frac{dvpv}{dt} > 0 \quad \text{when} \quad \mathcal{V}_{pv} < \mathcal{V}_M \quad (5)$$

$$\frac{d\mathcal{P}pv}{dt}\frac{dvpv}{dt} < 0 \quad \text{when} \quad \mathcal{V}_{pv} > \mathcal{V}_M \quad (6)$$

$$\frac{d\mathcal{P}pv}{dt}\frac{dvpv}{dt} = 0 \ \text{when} \quad \mathcal{V}_{pv} = \mathcal{V}_M \quad (7)$$

$$vpv = ipv\mathcal{R}_o(1-d)^2 \quad (8)$$

These observations result in the control law established in [16].

$$\frac{d\,dt}{dt} = k\frac{d\mathcal{P}pv}{dt}\frac{dvpv}{dt} \quad (9)$$

where the letter k represents a continuous loss of gain. It is possible to describe the regulation law (9) in a simple manner as follows: if v_{pV} rises and p_{pV} subsequently increases, the system's operating point is positioned to the left of the MPP see Figure. 1, necessitating a decrease in (d), which in turn will elevate v_{pV} as per (8); conversely, if p_{pV} diminishes following an increase in v_{pV}, Because the operational point of the system is located to the correct side of the MPP, as shown in Figure 1, it is necessary to raise d in order to reduce the value of v_{pV} via this process. In order to get maximum power, it is necessary to lower the time-dependent derivatives of d to zero. This may be accomplished by considering equations (7) and (9). RCC has been shown to have a solid theoretical basis and has been statistically confirmed to provide the optimal cycle of operation in maximizing power in the state of steady state. This is proved in [16], [17], [18], and [19]. RCC has an advantage over conventional algorithms such as P&O in that, under steady-state circumstances, RCC converges to the Maximum Power Point (MPP), while P&O oscillates about it. This is the fundamental difference between the two methods. When compared to fuzzy reasoning and neural networks, for example, RCC has several benefits, including the fact that it is easy to deploy and very inexpensive. The evaluation of the transient reaction of the boost converter's system, which is represented in Figure 2, is a key part of the steady-state study. This evaluation enables the controller to rapidly converge to the predicted maximum power point without not many oscillations.

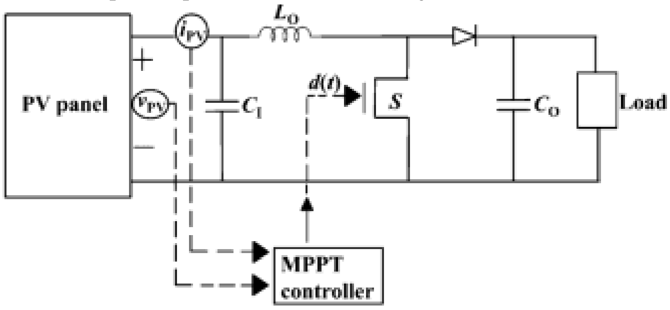

FIGURE. 2. MPPT controller implemented within of a PV boost converter system.

This control law requires simply time derivatives, which are expected to be easily used inside a system that really exists. The change is doable if dz/dt is nonzero, excluding the integral is not affected by isolated points that are isolated. Particularly, if the converter runs with a duty cycle on a continuously constant basis **[$D \epsilon (0,1)$]** and a switching period **[$T > 0$]**, With the exception of the switching edges, the product of state variables, which include currents and currents, will be nonzero throughout the switching process. in addition to providing suitable alternatives for z. It has been suggested that there are several approximations to the number four, each of which requires just the minimum of one multiplier. In converters that convert DC to DC, it is known to be piecewise constant rather commonly. dJ/dt Provided the sign information is sufficient, a synchronous demodulator may be employed. This method calculates $\mathcal{J}$ (often through multiplication), whereas dz/dt is ascertained using a filter and analogy switches governed by ***sgn***(dz/dt), which defines an integrand analogous to (4). An alternative approach is to focus solely on the phase of information [66], [89]. Within this concept indicates that RCC is analogous to a phase-locked loop. From a theoretical standpoint, it is possible to combine the two simplifications, in which case the integrand is approximated as ***sgn*** $({}^{dJ}/_{dt})$ ***sgn*** $({}^{dz}/_{dt})$. Due to the fact that important information has been left out, these approximations have an effect on sound defences, convergence rate, and perhaps the equilibrium value. Up to this point, RCC has been carried out by means of analogy circuitry. Derivatives of time may be obtained with relative ease. The derivation function is frequently replaced by a filter that has a gain that decreases dramatically beyond the frequency band of interest, typically at the frequency of switching. This is being done in order to improve the noise immunity of the system. Multiplication may be made easier with the help of an analogy multiplier from the AD633 family. Conventional analogy multipliers, which are created using bipolar technology, are characterized by rather high bias currents. This is disappointing. Under some circumstances, the Analog Devices AD633 has a power consumption of 120 milliwatts. The applications of power electronics provide several opportunities for energy optimization. Optimal efficiency can be achieved by adjusting the deadtime of the DC-DC converter [64], [65] or the flux magnitude of the induction motor [57]– [63]. Optimal efficacy can be achieved by adjusting active filters [66]. The majority of alternative energy sources possess a certain operating point that produces either optimal efficiency or maximum power. Photovoltaic (PV) cells must maintain their optimal power point, achieved by the regulation of maximum power point tracking, often known as MPPT. Several different algorithms for MPPT have been developed, and each one has a different amount of complexity [67]. These algorithms have been implemented in both the analogy and digital sectors. In the realm of switching power converters, ripple correlation control (RCC) represents a real-time optimization approach that has been particularly built for applications. The objective of an application known as maximum power point tracking, or MPPT, is to optimize the cost function, which may include the amount of power or energy that is produced. With respect to the cost function, the gradient is assessed by RCC using data from the inherent switching ripple. The outcome is that the control system can achieve a gradual time scale aim and operate at optimal levels due to the data on rapid variations in current and voltage. RCC has been utilized to tackle the MPPT challenge [68]–[77], improve motor efficiency [68], [78]– [83], reduce deadtime [68], [84], [85], and modify filters [66]. Ripple correlation control (RCC) is extended into the discrete-time domain by discrete-time ripple correlation control (DRCC) [86], [87].

III.PID CONTROLLERS

PID controllers, which stand for proportional-integral-derivative controllers, are the most well-known controllers used in industrial process control. This is because of its clear design and dependable performance over a wide range of operating conditions. All three types of gain proportional, integral, and derivative—have an impact on the controller design. The most major drawback is the amount of effort that must be spent improving the choice of controller settings [91]. Power Factor Correction (PFC) circuits exhibit inherently nonlinear dynamics, rendering conventional linear control strategies inadequately when optimal transient behaviour is demanded under varying operating conditions. This constraint can be mitigated by adjusting the gains of the controller that are proportional, integral, and derivative respectively to correspond with the revised operating conditions. The Ziegler–Nichol’s method is a commonly utilized technique for adjusting these improvements. Tuning formula is the best-recognized tuning procedure [90].

subsystems: A. Modelling of PID Controller

"The PID controller can be characterized by the following transfer function representation:"

$$\boldsymbol{G(s) = K_p + \frac{K_1}{s} + K_d s} \qquad \textbf{(10)}$$

The discrete-time representation of PID control utilized in this paper is expressed as

$$\textbf{u(k)}= \boldsymbol{K_p e(k) + K_i T_s \sum_{i=1}^{n} e(1) + \frac{K_d}{T_s} \Delta e(k)} \qquad \textbf{(11)}$$

"Within this framework, u(k) corresponds to the control input, while e(k) represents the deviation between the desired reference value and the actual system output. The variable T denotes the controller’s sampling interval. "

$$\Delta \boldsymbol{e(k) = e(k) - e(k-1)} \qquad \textbf{(12)}$$

It is possible to produce a wide range of dynamic response characteristics for a certain process by setting the PID gains, including the corresponding increase Kp, the integral gain Ki, and derivative gains Kd΄E.

Continuous monitoring of the DC connection voltage is performed, and the results are compared to a predetermined reference value. The Proportional-Integral-Derivative (PID) controller regulates the error signal and ensures its proper functioning. With its output constrained by a limiter to define the maximum reference current for the inductor. The peak value is then modulated using a rectified sinusoidal template, synchronized with the AC mains, to generate the corresponding reference current waveform. During the process of generating the gating signal for the switching mechanism of the converter, an hysteresis current controller (HCC) performs a comparison between the reference inductor current and the actual inductor current. Even in the presence of nonlinear load circumstances brought about by an inverter-driven switching reluctance motor (SRM) with variations in input supply voltage, the converter is able to maintain a steady DC link voltage thanks to the feedback mechanism. Furthermore, it ensures a sinusoidal current demand from the grid with a near unity power factor. For the purpose of delivering power to the switching reluctance motor (SRM), the pulse-width modulation (PWM) inverters is used. This inverter supplies alternating current (AC) voltage at varying frequencies, which are determined by the position feedback of the rotor. [93] A PID controller is responsible for controlling the rotational speed of the motor. This controller makes adjustments to the control signal in order to bring the actual speed into alignment with the intended reference. Before the reference current is created, this signal is restricted in its signal transmission. The reference and actual motor currents are supplied to a hysteresis current controller, which generates the gate signals for the inverter's IGBT switches. The signals are then adjusted according to rotor position to accommodate the SRM's nonlinear magnetic properties. The phase current and torque values, which are significantly influenced by rotor angle, are estimated using precomputed lookup tables [92].

IV.MATHEMATICALMODELLINGOFSRM

Switched reluctance motors (SRMs) are more economical than permanent magnet motors since they do not include a rotor and feature a simple field winding. Switched reluctance motors the is market for electrical drives and sees an increase in demand for motors as a consequence of their ability to produce significant torque, achieve high rotational speeds, and maintain efficiency. The adoption of SRM drive applications has surged in recent years due to their swift operational capabilities, appropriateness for hazardous environments, high torque/inertia ratio, and simple mechanical design [94],[95],[96]. The motor's principal deficiency is its significant torque ripple and highly nonlinear torque characteristics, leading to vibrations and noise. Prior discussions have examined several ways for alleviating torque disturbance [97]. In fluctuating load scenarios, torque-induced disturbances pose challenges for speed control. A proportional-integral controller has been applied in this investigation to mitigate these effects and maintain velocity stability. The switching reluctance motor under varying load conditions [98]. The motor's current, position, and velocity provide feedback signals. The motor drive sector is witnessing heightened interest in switching reluctant motors (SRMs) owing to their fault-tolerant attributes and durable design. The independent nature of torque generation at different stages is the basis of the essential fault-tolerant capability. The predominant converter topologies employed in switching reluctance motor drives exhibit resistance to shoot-through failures.

The defect tolerance of the complete motor driving system is enhanced by the elimination of permanent magnets. The reliance on rotor angle and phase current characteristics primarily causes the nonlinear nature of torque generation in SRM drives. Even though many fault-tolerant strategies have been suggested, techniques like current profiling and keeping unaffected phases on for longer only provide limited help and have significant drawbacks. Numerous systems neglect to account for dynamic fluctuations in machine parameters, instead depending on offline data gathered under static conditions. Moreover, most approaches are confined to velocities much below the motor's nominal speed and cannot provide torque with diminished ripple during fault conditions.

The efficacy of the SRM is profoundly affected by its magnetic configuration; thus, an elucidation of the principle of magnetic flux distribution is essential. The updated pole design formula defines the appropriate number of rotor poles required for optimal machine performance. Conventional Switched Reluctance Motors (SRMs) include a single tooth per stator pole to enable magnetic flux flow [100],[101],[102],[103], however, the suggested design has two teeth per pole to improve flux distribution. Two sets of teeth collectively enhance flow variation and reduce the duration of variation. Figures 3 Sequential functioning with the Switched Reluctance Motor (SRM)

(a) During the excitation phase, the rotor is aligned with the stator poles of phase c.

(b) The rotor moved and become aligned with the poles within the stator and phase a.

following commutation. depict a comparison between conventional topology and two-teeth topology. This architecture can produce enhanced transient torque output. Switched Reluctance Motors (SRMs) comprise laminated steel cores In a Both the stator and the rotor within a Switched Reluctance Motor (SRM) correspondingly are constructed with salient poles; however, only the stator poles are equipped with windings, while the rotor consists of laminated ferromagnetic teeth devoid of any windings or electrical conductors. Unlike induction or brushless DC (BLDC) motors, where the rotor participates in electromagnetic energy conversion through induced or permanent magnet excitation, the SRM rotor operates purely through variations in magnetic reluctance within the air gap [99]. The fundamental SRM was founded on the notion of decreasing magnetic reluctance, which is its working principle. by aligning the rotor poles with the stator poles that are currently energized. This mechanism is functionally analogous to that of BLDC motors in terms of sequential commutation, yet fundamentally distinct in construction. While BLDC motors utilize rotor embedded with permanent magnets to generate continuous torque, SRMs rely entirely on the saliency of the rotor to achieve torque production via reluctance alignment.

Figure 3 illustrates the electromechanical interaction within the SRM topology. Initially, consider that rotor poles r_1 and r_1' are in alignment with the energized stator poles c and $c^{'}$, while the remaining rotor poles are in proximity to stator poles a and a‘. When excitation is switched from phase a and $a^{'}$, the magnetic field induces a torque that causes rotor poles r_2 and r_2' to align with the newly energized stator poles. As the rotor continues to rotate, r_1 and r_1' will approach stator poles b and $b^{'}$. Subsequent excitation of phase b and $b^{'}$, further advances the rotor r_1 and r_1', completing one segment of the switching cycle. This stepwise commutation is synchronized with rotor position feedback to ensure efficient torque production and directional control. These two phases generate a clockwise rotational motion of the rotor. An SRM operates by replacing the motor using the same technique, which involves utilizing the rotor's position feedback.

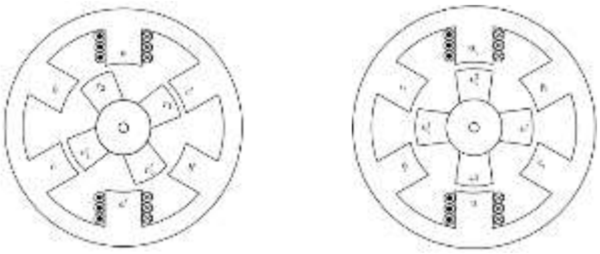

(a) (b)

FIGURE. 3. Sequential operation of the Switched Reluctance Motor (SRM)

Assuming negligible between phases, the SRM can be conveyed as the mutual inductance between phases. using a simplified equivalent circuit. The voltage across a given phase winding is defined accordingly:

$$v = R_S i + \frac{d\lambda(\theta,i)}{dt} \quad (1)$$

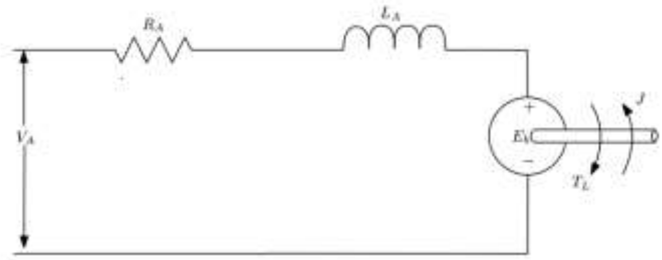

FIGURE. 4. Circuit of SRM which is comparable to a single phase

Where R_S represents the per-phase resistance, and λ denotes the flux linkage corresponding to each phase. The flux linkage is defined as follows:

$$\lambda(\theta,i) = L(\theta,i)i \quad (2)$$

Where L denotes the inductance, which varies as a function of both the phase current and rotor position. The governing equation for the phase voltage is expressed as:

$$v = Ri + L(\theta,i)\frac{di}{dt} + i\frac{d\theta}{dt}\frac{dL(\theta,i)}{d\theta} \quad (3)$$

$$= R_S i + L(\theta,i)\frac{di}{dt} + i w_m \frac{dL(\theta,i)}{d\theta} \quad (4)$$

The induced electromotive force, e, is subsequently derived as follows:

$$e = \frac{dL(\theta,i)}{dt} w_m i \quad (5)$$

$$= K_b w_m i \quad (6)$$

where K_b denotes the electromotive force constant and is defined as follows:

$$K_b = \frac{dL(\theta,i)}{dt} \quad (7)$$

The coefficient bis K_b dependent on the operating point and can be assessed at a fixed current for the corresponding position. In Figure 2, the single-phase equivalent circuit of the SRM is illustrated by utilizing the voltage relation in equation (4) and the induced electromotive force (EMF) expression in equation (5). It is possible to determine the power output by employing the subsequent formula:

$$p_i = vi = R_S i^2 + i^2\frac{d(\theta,i)}{dt} + L(\theta,i)i\frac{di}{dt} \quad (8)$$

The concluding phrase in (8) is expressed using established variables to facilitate a significant inference.

$$\frac{d}{dt}\left(\frac{1}{2}L(\theta,i)i^2\right) = L(\theta,i)i + \frac{1}{2}i^2\frac{dL(\theta,i)}{dt} \quad (9)$$

By substituting the appropriate variables into the power equation (8), the resulting expression quantifies the instantaneous power output of the system. This substitution facilitates the analysis of power flow within the SRM phase circuit under varying operating conditions, enabling more accurate modelling and control design.

$$p_i = R_S i^2 + L(\theta,i)i + \frac{1}{2}i^2\frac{dL(\theta,i)}{dt} \quad (10)$$

Within this context, (p_i) signifies the instantaneous input power. The total amount of resistivity losses, the variability in magnetic field energy over time, and the power of the air gap are the components that make up the input power. (p_a), mathematically denoted by the expression$(L(\theta,i)\frac{i^2}{2})$. The rotor speed is thereafter articulated using the following equation:

$$w_m = \frac{d\theta}{dt} \quad (11)$$

The power delivered through the air gap manifests as...

$$p_a = \frac{1}{2}i^2\frac{dL(\theta,i)}{d\theta}\frac{d\theta}{dt} \quad (12)$$

$$= w_m T_e \quad (13)$$

As a consequence of this, the electromagnetic torque can potentially be mathematically characterized by the sentence that follows:

$$T_e = \frac{1}{2}i^2\frac{dL(\theta,i)}{d\theta} \quad (14)$$

A discussion on the estimate of torque in switching reluctance motors (SRMs) is included in this article. One of the most significant challenges that must be overcome in order to create control mechanisms for SRMs is the lack of a mechanism that is both accurate and reliable for estimating torque. As a result of this gap, various research efforts have been forced to rely on already present references files for torque-current-position connections or on mathematical models that are too simplified and fail to adequately describe the complex nonlinearities that are inherent in the behaviour of this particular kind of motor. Whether they are inefficient in high-performance applications or hold an excessive amount of complexity, the control methods that have been presented either prevent their implementation in real time or are inefficient.

In order to achieve optimum adjustment of current waveforms while the device is in operation, it is necessary to have a correlation that is both exact and realistic between the required current and the torque that is planned. The production of torque in switched reluctance motors (SRMs) is a complex process since it is dependent not only on the position of the rotor but also on the strength of the current. As a result, it is difficult to directly correlate current and torque using a straightforward formula. Therefore, it is very necessary to make use of numerical solutions in order to determine the necessary currents in compliance with the torque parameters. The use of a torque controller that makes use of the analytical model described in reference [104], [105], and [106] has been carried out in this particular setting. This particular controller is differentiated by its ability to adapt to changes in the parameters of the motor; thus, it enhances the accuracy of traction control in a system that operates in a closed-loop configuration. In addition, a continuous function is used to illustrate the link between the magnetic flux and the current phase for this specific type of motor. This function contributes to the accurate description of the magnetic characteristics that are required for an accurate and efficient torque calculation.

$$\boldsymbol{\psi_k = \psi_s\left(1 - e^{-f_{\mathcal{K}}(\theta) i_{\mathcal{K}}}\right),\ i_{\mathcal{K}} \geq 0} \qquad (15)$$

Flux saturation in the winding is reflected in the localized regions of the magnetic path where the flux linkage ceases to increase linearly. The corresponding phase current and the flux linkage curvature, as a function of rotor position, are modelled via a Fourier series to capture these nonlinear behaviours accurately.

$$\boldsymbol{f_k(\theta) = a_0 + \sum_{m=1}^{\infty} a_m \cos\left(m\left(\theta - (k-1)\frac{2\pi}{\mathcal{N}_{ph}}\right)\right) + b_m \sin\left(m\left(\theta - (k-1)\frac{2\pi}{N_{ph}}\right)\right)}$$

The expression for the phase torque, as given in equation (16), is derived based on the Fourier decomposition of the magnetic characteristics and the instantaneous electrical position of the rotor.

$$\boldsymbol{T_k = \frac{\psi_s \frac{df_k(\theta)}{d(\theta)}}{f_k^2(\theta)}\left[1 - (1 + i_k f_k(\theta)) e^{-i_k f_k(\theta)}\right]} \qquad (16)$$

Torque estimation is carried out via equation (2), with the machine's inductance characteristics being identified dynamically during operation [105], [106]. The torque observer supplies phase-resolved torque data in real time, enabling accurate monitoring of both individual and total torque outputs.

RESULTS AND DISCUSSION

The ultimate loader was a single-phase reluctance motor (SRM), and a simulation of the suggested control system was performed. This system integrates the Ripple Correlation Control (RCC) algorithm with a PID controller. The evaluation was divided into three testing stages to check how well the system works in different conditions, such as changes in sunlight and speed.

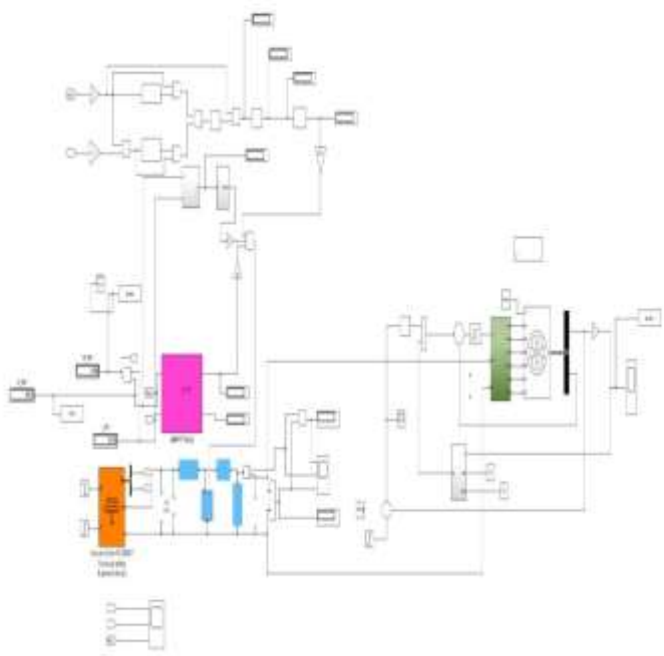

FIGURE. 5. BLOCK DIAGRAM OF RCC, PID AND SRM Phase One: Standard Operations

During this phase, the motor speed was sustained at 400 rpm, and the solar radiation level was fixed at 800 W/m². The system showed it could accurately track the maximum power point (MPP), showing much less variation because of the control circuits and very stable voltage and current.

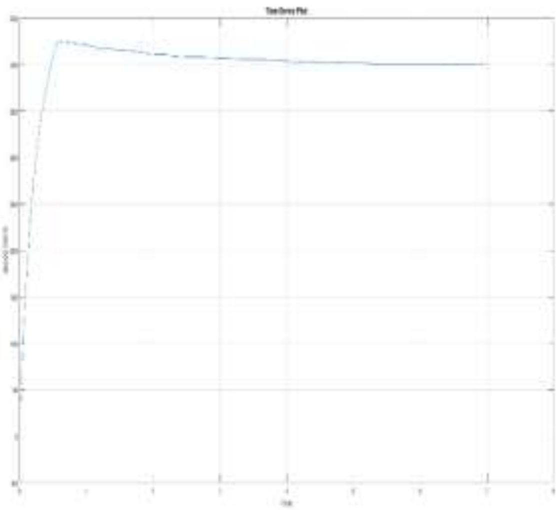

FIGUER. 6. CONSTANT SPEED 400 RPM WITH CONSTANT IRRADIANCE 800 W/m²

Phase Two: Velocity Fluctuation

The sun irradiation was sustained at 800 W/m², and the engine's velocity was decreased to 200 rpm. The system exhibited an efficient dynamic reaction to fluctuating mechanical loads. Even though the speed was lower, the RCC algorithm and the PID controller quickly adjusted the system to keep it working efficiently and still collect energy well.

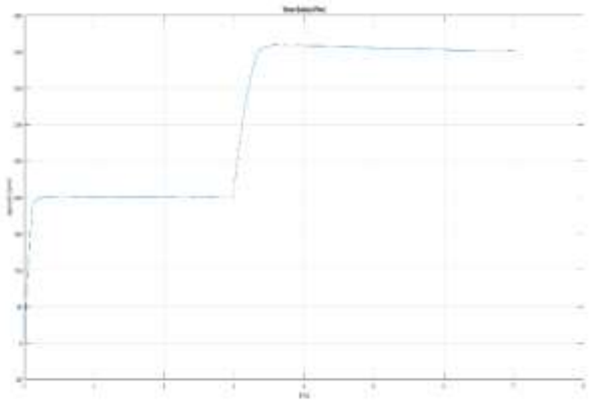

FIGUER. 7. CHANGE SPEED TO 200 RPM WITH CONSTANT IRRADIANCE 800 W/m²

Phase 3: Modification in Solar Irradiance
In this phase, solar radiation was reduced to 600 W/m², and the motor speed was reinstated at 400 rpm. The system's adaptability to changing environmental circumstances was shown by the findings, which indicated its outstanding flexibility in monitoring the ideal power point and modifying the current and voltage in response to reduced irradiance.

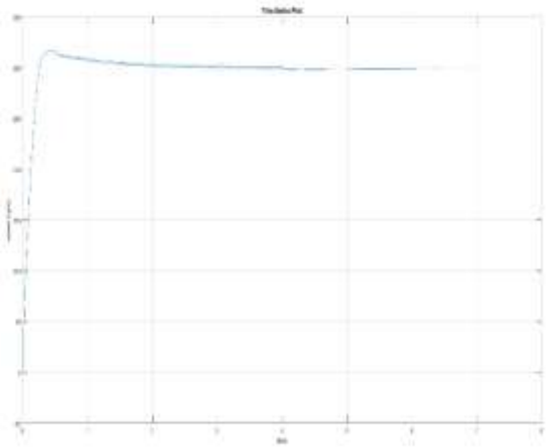

FIGUER. 8. SPEED CONSTANT IN 400 RPM AND THE PV IRRADIANCE CHANGING FROM 800 TO 600 W/m²

The system consistently performed and tracked accurately in a variety of operating conditions, underscoring its overall effectiveness. This highlights the possibility of the RCC algorithms in power management applications for motors powered by sources of renewable energy when integrated with PID.

CONCLUSIONS

This study has established Ripple Correlation Control (RCC) as an effective real-time optimization strategy for both photovoltaic maximum power point tracking (MPPT) and switched reluctance motor (SRM) drive applications. By harnessing the inherent switching-induced ripple and PWM dithering, RCC enables efficient extremum-seeking behaviours without the drawbacks associated with conventional perturbative or model-dependent methods. The integration of RCC within a two-tier control architecture—combining proportional-integral-derivative (PID) control for steady-state precision with model reference adaptive control (MRAC) for dynamic compensation—demonstrates improved tracking speed, reduced oscillations, and enhanced robustness against system nonlinearities and parameter variations. In the context of SRM drives, RCC complements the machine's intrinsic fault-tolerant capabilities and nonlinearity, contributing to improved torque regulation and reduced ripple. Furthermore, the comparative analysis of PID-based controllers for brushless permanent magnet DC (BLPMDC) motors reaffirms the utility of digital and auto-tuned implementations in achieving low overshoot, minimized steady-state error, and fast dynamic response. Overall, the proposed RCC-based control paradigm presents a scalable, low-complexity, and adaptive solution for modern power electronic systems. Its applicability across diverse domains—ranging from renewable energy systems to electric motor drives—underscores its potential as a unified control framework for high-performance, real-time applications under dynamic operating conditions.

REFERENCES

1. S. L. Brunton, C. W. Rowley, S. R. Kulkarni, and C. Clarkson, “Maximum power point tracking for photovoltaic optimization using ripple-basedextremum seeking control,” IEEE Trans. Power Electron., vol. 25,no. 10, pp. 2531–2540, Oct. 2010.
2. R. A. Mastromauro, M. Liserre, T. Kerekes, and A. Dell’Aquila, “A singlephase voltage-controlled grid connected photovoltaic system with power quality conditioner functionality,” IEEE Trans. Ind. Electron., vol.56, no. 11, pp. 4436–4444, Nov. 2009
3. A. K. Abdelsalam, A. M. Massoud, S. Ahmed, and P. N. Enjeti,“High-performance adaptive perturb and observe MPPT technique for photovoltaic-based microgrids,” IEEE Trans. Power Electron., vol. 26,no. 4, pp. 1010–1021, Apr. 2011.
4. M. A. Elgendy, B. Zahawi, and D. J. Atkinson, “Assessment of perturb and observe MPPT algorithm implementation techniques for PV pumping applications,” IEEE Trans. Sustainable Energy, vol. 3, no. 1, pp. 21–33, Jan. 2012.
5. G. Petrone, G. Spagnuolo, and M. Vitelli, “A multivariable perturb-andobserve maximum power point tracking technique applied to a singlestage photovoltaic inverter,” IEEE Trans. Ind. Electron., vol. 58, no. 1, pp. 76–84, Jan. 2011.
6. S. Jain and V. Agarwal, “A new algorithm for rapid tracking of approximate maximum power point in photovoltaic systems,” IEEE Power Electron. Lett., vol. 2, no. 1, pp. 16–19, Mar. 2004.

7. M. de Brito, L. Galotto, L. Sampaio, G. de Azevedo e Melo, and C. Canesin, “Evaluation of the main MPPT techniques for photovoltaic applications,” IEEE Trans. Ind. Electron., vol. 60, no. 3, pp. 1156–1167, Mar. 2013.
8. T. Esram and P. Chapman, “Comparison of photovoltaic array maximum power point tracking techniques,” IEEE Trans. Energy Convers., vol. 22, no. 2, pp. 439–449, Jun. 2007.
9. P. T. Krein, “Ripple correlation control, with some applications,” in Proc. IEEE Int. Symp. Circuits Syst., 1999, pp. 283–286.
10. [10] A. M. Bazzi and P. T. Krein, “Ripple correlation control: An extremum seeking control perspective for real-time optimization,” IEEE Trans. Power Electron., vol. 29, no. 2, pp. 988–995, Feb. 2014.
11. R. Leyva, C. Alonso, I. Queinnec, A. Cid-Pastor, D. Lagrange, and L. Martinez-Salamero, “Maximum power point tracking of photovoltaic systems using extremum-seeking control,” IEEE Trans. Aerosp. Electron. Syst., vol. 42, no. 1, pp. 249–258, Jan. 2006.
12. J. W. Kimball and P. T. Krein, “Discrete-time ripple correlation control for maximum power point tracking,” IEEE Trans. Power Electron., vol. 23, no. 5, pp. 2353–2362, Sep. 2008.
13. C. Barth, and R. C. N. Pilawa-Podgurski, “Dithering digital ripple correlation control for photovoltaic maximum power point tracking,” in Proc. IEEE Power Energy Conf., 2013, pp. 36–41.
14. T. Esram, J. W. Kimball, P. T. Krein, P. L. Chapman, and P. Midya,“Dynamic maximum power point tracking of photovoltaic arrays using ripple correlation control,” IEEE Trans. Power Electron., vol. 21, no. 5,pp. 1282–1291, Sep. 2006.
15. N. Femia, G. Petrone, G. Spagnuolo, and M. Vitelli, “Optimization of perturb and observe maximum power point tracking method,” IEEE Trans. Power Electron., vol. 20, no. 4, pp. 963–973, Jul. 2005.
16. P. T. Krein, “Ripple correlation control, with some applications,” in Proc. IEEE Int. Symp. Circuits Syst., 1999, vol. 5, pp. 283–286.
17. D. L. Logue and P. T. Krein, “Optimization of power electronic systems using ripple correlation control: A dynamic programming approach,” in Proc. IEEE 32nd Annu. Power Electron. Special. Conf., 2001, vol. 2, pp. 459–464.
18. J. W. Kimball and P. T. Krein, “Discrete-time ripple correlation control for maximum power point tracking,” IEEE Trans. Power Electron., vol. 23, no. 5, pp. 2353–2362, Sep. 2008.
19. T. Esram, J. W. Kimball, P. T. Krein, P. L. Chapman, and P. Midya, “Dynamic maximum power point tracking of photovoltaic arrays using ripple correlation control,” IEEE Trans. Power Electron., vol. 21, no. 5, pp. 1282–1291, Sep. 2006
20. D. E. Miller, “A new approach to model reference adaptive control,” IEEE Trans. Autom. Control, vol. 48, no. 5, pp. 743–757, May 2003.
21. S. Sastry and M. Bodson, Adaptive Control: Stability, Convergence and Robustness. New York: Dover Publications, 2011.
22. T. J. E. Miller, Switched Reluctance Motors and Their Control. Oxford, U.K.: Oxford Science, 1993
23. B. L. G. Costa, C. L. Graciola, B. A. Angélico, A. Goedtel, and M. F. Castoldi, ‘‘Metaheuristics optimization applied to PI controllers tuning of a DTC-SVM drive for three-phase induction motors,’’ Appl. Soft Comput., vol. 62, pp. 776–788, Jan. 2018.
24. A. M. Khambadkone and J. Holtz, ‘‘Compensated synchronous PI current controller in overmodulation range and six-step operation of spacevector-modulation-based vector-controlled drives,’’ IEEE Trans. Ind. Electron., vol. 49, no. 3, pp. 574–580, Jun. 2002.
25. Z. Ibrahim and E. Levi, ‘‘A comparative analysis of fuzzy logic and PI speed control in high-performance AC drives using experimental approach,’’ IEEE Trans. Ind. Appl., vol. 38, no. 5, pp. 1210–1218, Sep. 2002.
26. D. Zhang, H. Li, and E. G. Collins, ‘‘Digital anti-windup PI controllers for variable-speed motor drives using FPGA and stochastic theory,’’ IEEE Trans. Power Electron., vol. 21, no. 5, pp. 1496–1501, Sep. 2006.
27. A. Ma'arif and N. R. Setiawan, "Control of DC motor using integral state feedback and comparison with PID: simulation and arduino implementation," Journal of Robotics and Control (JRC), vol. 2, no. 5, pp. 456-461, 2021.
28. M. Khalifa, AL H. Amhedb, and M. Al Sharqawi, "Position Control of Real Time DC Motor Using LabVIEW," Journal of Robotics and Control (JRC), vol. 2, no. 5, pp. 342-348, 2021.
29. A. Ma'arif and A. Çakan, "Simulation and arduino hardware implementation of dc motor control using sliding mode controller," Journal of Robotics and Control (JRC), vol. 2, no. 6, pp. 582-587, 2021.
30. R. T. Yunardi, D. Arifianto, F. Bachtiar, and J. I. Prananingrum, "Holonomic implementation of three wheels omnidirectional mobile robot using dc motors," Journal of Robotics and Control (JRC), vol. 2, no. 2, pp. 65-71, 2021.
31. Y. I. Al Mashhadany, "High-performance multilevel inverter drive of brushless DC motor," International Journal of Sustainable and Green Energy, vol. 4, no. 3-1, pp. 1-7, 2015.
32. S. W. Shneen, D. H. Shaker, and F. N. Abdullah, "Simulation model of PID for DC-DC converter by using MATLAB," International Journal of Electrical

and Computer Engineering, vol. 11, no. 5, p. 3791, 2021.

33. R. M. Pindoriya, et al., "Comparative analysis of permanent magnet motors and switched reluctance motors capabilities for electric and hybrid electric vehicles," 2018 IEEMA Engineer Infinite Conference (eTechNxT). IEEE, pp. 1-5, 2018.
34. A. E. Aliasand, and F. T. Josh, "Selection of motor foran electric vehicle: A review," Materials Today: Proceedings, vol. 24, pp. 1804-1815, 2020.
35. N. Milivojevic, et al., "Stability analysis of FPGA-based control of brushless DC motors and generators using digital PWM technique," IEEE transactions on industrial electronics, vol. 59, no. 1, pp. 343-351, 2011.
36. S. Hans, and S. Ghosh, "Position analysis of brushless direct current motor using robust fixed order H-infinity controller," Assembly Automation, vol. 40, no. 2, pp. 211-218, 2020.
37. V. Madonna, et al., "The rebirth of the current source inverter: Advantages for aerospace motor design," IEEE Industrial Electronics Magazine, vol. 13, no. 4, pp. 65-76, 2019.
38. D. H. Shaker, S. W. Shneen, F. N. Abdullah, and G. A. Aziz, "Simulation Model of Single-Phase AC-AC Converter by Using MATLAB," Journal of Robotics and Control (JRC), vol. 3, no. 5, pp. 656-665, 2022.
39. X. Ding, Y. Zhou, and J. Cheng, "A review of gallium nitride power device and its applications in motor drive," CES Transactions on Electrical Machines and Systems, vol. 3, no. 1, pp. 54-64, 2019.
40. M. Galea et al., "Reliability-Oriented Design of Electrical Machines: The Design Process for Machines' Insulation Systems MUST Evolve," IEEE Industrial Electronics Magazine, vol. 14, no.1, pp. 20-28, 2020.
41. X. F. Zheng, et al., "A review of thermoelectrics research–Recent developments and potentials for sustainable and renewable energy applications," Renewable and Sustainable Energy Reviews, vol. 32, pp. 486-503, 2014.
42. J. C. Najmon, S. Raeisi, and A. Tovar, "Review of additive manufacturing technologies and applications in the aerospace industry," Additive manufacturing for the aerospace industry, pp. 7-31, 2019.
43. H. S. Dakheel, Z. B. Abdullah, N. S. Jasim, and S. W. Shneen, "Simulation model of ANN and PID controller for direct current servo motor by using Matlab/Simulink," Telkomnika, vol. 20, no. 4, 2022.
44. J. Feng, K. Liu, and Q. Wang, "Scheme based on buck-converter with three-phase H-bridge combinations for high-speed BLDC motors in aerospace applications," IET Electric Power Applications, vol. 12, no. 3, pp. 405-414, 2018.
45. W. Chen et al., "A novel method of reducing commutation torque ripple for brushless DC motor based on Cuk converter," IEEE Transactions on Power Electronics, vol. 32, no. 7, pp. 5497-5508, 2016.
46. X. Zhou et al. "Fast commutation instant shift correction method for sensorless coreless BLDC motor based on terminal voltage information," IEEE Transactions on Power Electronics, vol. 32, no. 12, pp. 9460-9472, 2017.
47. H. A. Toliyat and T. Gopalarathnam, "AC machines controlled as DC machines (Brushless DC machines/electronics)," The power electronics handbook, CRC Press, 2018.
48. S. W. Shneen, F. N. Abdullah, and D. H. Shaker, "Simulation model of single phase PWM inverter by using MATLAB/Simulink," International Journal of Power Electronics and Drive Systems, vol. 12, no. 1, p. 212, 2021.
49. X. Xiang, J. Chai, and X. Sun, "A novel DC motor based on mechanical–electrical hybrid commutation," IEEE Journal of Emerging and Selected Topics in Power Electronics, vol. 6, no. 3, pp. 1605-1615, 2017.
50. R. Ramachandran, D. Ganeshaperumal and B. Subathra, "Closedloop Control of BLDC Motor in Electric Vehicle Applications," 2019 IEEE International Conference on Clean Energy and Energy Efficient Electronics Circuit for Sustainable Development (INCCES), pp. 1-5, 2019.
51. B. Alsayid, W. A. Salah, and Y. Alawneh, "Modelling of sensored speed control of BLDC motor using MATLAB/SIMULINK," International Journal of Electrical and Computer Engineering, vol. 9, no. 5, pp. 3333-3343, 2019.
52. A. A. El-Samahy and M. A. Shamseldin, "Brushless DC motor tracking control using self-tuning fuzzy PID control and model reference adaptive control," Ain Shams Engineering Journal, vol. 9, no. 3, pp. 341-352, 2018.
53. S. W. Shneen, et al., "Application of LFAC {16 2/3Hz} for electrical power transmission system: a comparative simulation study," TELKOMNIKA (Telecommunication Computing Electronics and Control), vol. 17, no. 2, pp. 1055-1064, 2019.
54. A. Azarudeen and D. Mary, "Performance analysis of conventional and digital PWM control scheme for speed control of BLDC motor drives," 2017 International Conference on Advances in Electrical Technology for Green Energy (ICAETGT), pp. 69-75, 2017.
55. K. S. Devi, R. Dhanasekaran and S. Muthulakshmi, "Improvement of speed control performance in BLDC motor using fuzzy PID controller," 2016 International Conference on Advanced Communication Control and Computing Technologies (ICACCCT), pp. 380-384, 2016.

56. M. A. Shamseldin and A. A. EL-Samahy, "Speed control of BLDC motor by using PID control and self-tuning fuzzy PID controller," 15th International Workshop on Research and Education in Mechatronics (REM), pp. 1-9, 2014.
57. F. Abrahamsen, F. Blaabjerg, J. K. Pedersen, and P. B. Thoegersen, “Efficiency-optimized control of medium-size induction motor drives,” IEEE Trans. Ind. Appl., vol. 37, no. 6, pp. 1761–1767, Nov./Dec. 2001.
58. M. E. H. Benbouzid and N. S. N. Said, “An efficiency-optimization controller for induction motor drives,” IEEE Power Eng. Rev., vol. 18, no. 5, pp. 63–64, May 1998.
59. C. Chakraborty and Y. Hori, “Fast efficiency optimization techniques for the indirect vector-controlled induction motor drives,” IEEE Trans. Ind. Appl., vol. 39, no. 4, pp. 1070–1076, Jul./Aug. 2003.
60. I. Choy, S. H. Kwon, J. Y. Choi, J. W. Kim, and K. B. Kim, “On-line efficiency optimization control of a slip angular frequency-controlled induction motor drive using neural networks,” in Proc. IEEE Int. Conf. Ind. Electron., Control, Instrum., 1996, pp. 1216–1221.
61. T. C. Huang and M. A. El-Sharkawi, “Induction motor efficiency maximizer using multi-layer fuzzy control,” in Proc. Int. Conf. Intell. Syst. Appl. Power Syst., 1996, pp. 109–113.
62. M. W. Turner, V. E. McCormick, and J. G. Cleland, “Efficiency optimization control of AC induction motors: Initial laboratory results,” Environmental Protection Agency, EPA/600/SR-96/008, May 1996.
63. J. B. Wang and C. M. Liaw, “Indirect field-oriented induction motor drive with fuzzy detuning correction and efficiency optimisation controls,” IEE Proc. Elec. Power Appl., vol. 144, no. 1, pp. 37–45, Jan. 1997.
64. J. A. A. Qahouq, H. Mao, H. J. Al-Atrash, and I. Batarseh, “Maximum efficiency point tracking (MEPT) method and digital dead time control implementation,” IEEE Trans. Power Electron., vol. 21, no. 5, pp. 1273–1281, Sep. 2006.
65. V. Yousefzadeh and D. Maksimovic, “Sensorless optimization of dead times in dc-dc converters with synchronous rectifiers,” IEEE Trans. Power Electron., vol. 21, no. 4, pp. 994–1002, Jul. 2006.
66. R. Balog and P. T. Krein, “Automatic tuning of coupled inductor filters,” in Proc. IEEE Power Electron. Specialists Conf., 2002, pp. 591–596.
67. T. Esram and P. L. Chapman, “Comparison of photovoltaic array maximum power point tracking techniques,” IEEE Trans. Energy Convers., vol. 22, no. 3, pp. 439–449, Jun. 2007.
68. P. T. Krein, “Ripple correlation control, with some applications,” in Proc. IEEE Int. Symp. Circuits Syst., 1999, pp. 283–286.
69. P. Midya, “Nonlinear control and operation of dc to dc switching power converters,” Ph.D. dissertation, Dept. Elect. Comput. Eng., Univ. Illinois Urbana-Champaign, Urbana-Champaign, 1995.
70. P. Midya, P. T. Krein, and R. J. Turnbull, “Self-excited power minimizer/maximizer for switching power converters and switching motor drive applications,” U.S. Patent 5 801 519, Sep. 1, 1998.
71. P. Midya, P. T. Krein, R. J. Turnbull, R. Reppa, and J. W. Kimball, “Dynamic maximum power point tracker for photovoltaic applications,” in Proc. IEEE Power Electron. Specialists Conf., 1996, pp. 1710–1716.
72. R. S. Reppa, “A maximum power point tracker for photovoltaic applications,” M.S. thesis, Dept. Elect. Comput. Eng., Univ. Illinois Urbana-Champaign, Urbana-Champaign, 1996.
73. T. Esram, “Maximum power point tracking of photovoltaic arrays using ripple correlation control,” M.S. thesis, Dept. Elect. Comput. Eng., Univ. Illinois Urbana-Champaign, Urbana-Champaign, 2004.
74. N. D. Benavides, T. Esram, and P. L. Chapman, “Ripple correlation control of a multiple-input dc-dc converter,” in Proc. IEEE Power Electron. Specialists Conf., 2005, pp. 160–164.
75. D. Casadei, G. Grandi, and C. Rossi, “Single-phase single-stage photovoltaic generation system based on a ripple correlation control maximum power point tracking,” IEEE Trans. Energy Convers., vol. 21, no. 3, pp. 562–568, Jun. 2006.
76. Y. H. Lim and D. C. Hamill, “Synthesis, simulation and experimental verification of a maximum power point tracker from nonlinear dynamics,” in Proc. Power Electron. Specialists Conf., 2001, pp. 199–204.
77. T. Esram, J. W. Kimball, P. T. Krein, P. L. Chapman, and P. Midya, “Dynamic maximum power point tracking of photovoltaic arrays using ripple correlation control,” IEEE Trans. Power Electron., vol. 21, no. 5, pp. 1282–1291, Sep. 2006.
78. D. L. Logue, “Power electronic building block applications in optimization, control, and simulation,” Ph.D. dissertation, Dept. Elect.Comput. Eng., Univ. Illinois Urbana-Champaign, Urbana-Champaign, 2000.
79. D. L. Logue and P. T. Krein, “Machine efficiency optimization using ripple correlation control,” in Proc. Appl. Power Electron. Conf., 2001, pp. 642–648.
80. D. L. Logue and P. T. Krein, “Optimization of power electronic systems using ripple correlation control: A dynamic programming approach,” in Proc. IEEE Power Electron. Specialists Conf., 2001, pp. 459–464.
81. D. L. Logue and P. T. Krein, “Observer-based techniques in ripple correlation control applied to power electronic systems,” in Proc. IEEE Power Electron. Specialists Conf., 2001, pp. 2014–2018.

82. J. R. Wells, P. L. Chapman, and P. T. Krein, “Applications of ripple correlation control of electric machinery,” in Proc. IEEE Int. Electric Mach. Drives Conf., 2003, pp. 1498–1503.
83. J. R. Wells, P. L. Chapman, and P. T. Krein, “Fundamental aspects of ripple correlation control of electric machinery,” in Proc. IEEE Power Electron. Specialists Conf., 2003, pp. 1659–1662.
84. J. W. Kimball and P. T. Krein, “Continuous-time optimization of gate timing for synchronous rectification,” in Proc. Midw. Symp. Circuits Syst., 1996, pp. 1015–1018.
85. [85] J. W. Kimball and P. T. Krein, “Real-time optimization of dead time for motor control inverterse,” in Proc. IEEE Power Electron. Specialists Conf., 1997, pp. 597–600.
86. [86] J. W. Kimball and P. T. Krein, “Digital ripple correlation control for photovoltaic applicationse,” in Proc. IEEE Power Electron. Specialists Conf., 2007, pp. 1690–1694.
87. [87] J. W. Kimball, “Digital control techniques for switching power converters,” Ph.D. dissertation, Dept. Elect. Comput. Eng., Univ. Illinois, Urbana, 2007.
88. [88] H. Patel and V. Agarwal, “MATLAB-based modeling to study the effects of partial shading on PV array characteristics,” IEEE Trans. Energy Convers., vol. 23, pp. 302–310, Mar. 2008.
89. R. Balog, “Coupled Inductor: A basic filter building block, analysis, simulation and examples,” M.S. thesis, Dept. Elect. Comput. Eng., Univ. Illinois Urbana-Champaign, Urbana-Champaign, 2002.
90. J. G. Ziegler and N.B. Nichols," Optimum settings for aytomatic controllers", Trans. ASME, Vol.64, pp. 759-768, 1942.
91. W. Leonhard, " Microcomputer control of high dynamic performance AC drives-a survey", Automatica 1986.
92. R. Krishnan, "Switch Reluctance Motor Drives modeling, simulation analysis design and applications," CRC press, 2001(Book).
93. V. K. Sharma, B. Singh, S. S. Murthy, "Dynamic Analysis of Sliding Mode Control of Switched Reluctance Motor Drive," IE(I) Journal-EL, Vol. 79, pp. 119-125, December 1998.
94. K. Vijayakumar, R. Karthikeyan, S. Paramasivam, R. Arumugam and K. N. Srinivas, ”Switched reluctance motor modeling design simulation and analysis: A comprehensive review”, IEEE Trans. Magn., vol. 44, no. 12, pp. 4605-4617, Dec. 2008.
95. Simulation of a 6/4 SRM Based on Matlab/Simulink Environment. F Soares, P.J. Costa Branco IEEE July 2001.
96. P. Chancharoensook and M.F. Rahman, “Dynamic Modeling of a four phase 8/6 Switched Reluctance Motor using Current and Torque Lookup tables,” IEEE Trans.Industrial Applications, pp.491-496, 2002.
97. X. Deng, B. Mecrow, H. Wu and R. Martin, ”Design and Development of Low Torque Ripple Variable-Speed Drive System With Six-Phase Switched Reluctance Motors,” in IEEE Transactions on Energy Conversion, vol. 33, no. 1, pp. 420-429, March 2018, doi:10.1109/TEC.2017.2753286.
98. Y. Xu, X. Wang, Z. Xu and Y. Zhang,”Analysis and Application of Control Strategy for Switched Reluctance Drive with Position Sensor,” 2019 IEEE 8th Joint International Information Technology and Artificial Intelligence Conference (ITAIC), 2019, pp. 1363-1367, doi: 10.1109/ITAIC.2019.8785465.
99. Dragan S. Mihic,Mladen V. Terzic,Slobodan N. Vukosavic,“A New Nonlinear Analytical Model of the SRM With Included Multiphase Coupling”IEEE Transactions on Energy Conversion,2017 doi:10.1109/TEC.2017.2707587
100. A. G. Jack, B. C. Mecrow, and J. A. Haylock, “A comparative study of permanent magnet and switched reluctance motors for high-performance fault-tolerant applications,” IEEE Trans. Ind. Applicat., vol. 32, pp. 889–895, July/Aug. 1996.
101. C. Hao and Z. Chao, “Analysis of electrical faults for switched reluctance motor driver,” in Proc. 3rd World Congr. Intell. Contr. Automat., 2000, pp. 666–669.
102. H. Chen, C. Zhang, and G. Xie, “Analysis of the four-phase switched reluctance motor drive under the lacking one phase fault condition,” in Proc. IEEE-APCCAS Annu. Meeting, Circuits Syst., 2000, pp. 304–308
103. L. A. Belfore and A. Arkadan, “A methodology for characterizing fault tolerant switched reluctance motors using neurogenetically derived models,” IEEE Trans. Energy Conv., vol. 17, pp. 380–384, Sept. 2002.
104. M. Ilic’-Spong, R. Marino, S. Peresada, and D. Taylor, “Feedback linearizing control of switched reluctance motors,” IEEE Trans. Automat. Contr., vol. AC-32, pp. 371–379, May 1987.
105. S. Mir, I. Husain, and M. Elbuluk, “Switched reluctance motor modeling with online parameter identification,” IEEE Trans Ind. Applicat., vol. 34, pp. 776–783, July/Aug. 1998.
106. S. Mir, M. S. Islam, T. Sebastian, and I. Husain, “Self-tuning of machine parameters in switched reluctance motor drives,” in Proc. 35th IEEE Ind. Applicat. Soc. Annu. Meeting, vol. 3, 2001, pp. 2081–2088.